



Measurement of the inelastic pp cross-section at a centre-of-mass energy of $\sqrt{s} = 7 \text{ TeV}$

The LHCb collaboration[†]

Abstract

The cross-section for inelastic proton-proton collisions, with at least one prompt long-lived charged particle of transverse momentum $p_T > 0.2 \text{ GeV}/c$ in the pseudo-rapidity range $2.0 < \eta < 4.5$, is measured by the LHCb experiment at a centre-of-mass energy of $\sqrt{s} = 7 \text{ TeV}$. The cross-section in this kinematic range is determined to be $\sigma_{\text{inel}}^{\text{acc}} = 55.0 \pm 2.4 \text{ mb}$ with an experimental uncertainty that is dominated by systematic contributions. Extrapolation to the full phase space, using PYTHIA 6, yields $\sigma_{\text{inel}} = 66.9 \pm 2.9 \pm 4.4 \text{ mb}$, where the first uncertainty is experimental and the second is due to the extrapolation.

Submitted to JHEP

© CERN on behalf of the LHCb collaboration, license CC-BY-4.0.

[†]Authors are listed at the end of this paper.

1 Introduction

The inelastic cross-section is a fundamental observable in high-energy hadronic interactions. It is also important in astroparticle physics for models of extensive air showers induced by cosmic rays in the atmosphere [1]. Currently, it is not possible to calculate its value from first principles because quantum chromodynamics cannot yet be solved for soft processes. Phenomenological models assume a rise of the inelastic cross-section with energy according to a power law [2,3], while not exceeding the Froissart-Martin bound [4,5], which is asymptotically proportional to $\ln^2 s$. Although originally the Froissart-Martin bound was derived for the total cross-section, later developments show that it is also valid for the inelastic cross-section [6].

Measurements of the inelastic proton-proton (pp) cross-section at $\sqrt{s} = 7$ TeV have been reported by the ALICE [7], ATLAS [8,9], CMS [10] and TOTEM [11,12] collaborations, using experimental information from the central (ALICE, ATLAS, CMS) and the extremely forward (ATLAS, TOTEM) regions. LHCb allows those results to be complemented by a measurement in the mid- to forward rapidity range $2.0 < \eta < 4.5$.

2 Detector description and data set

The LHCb detector [13] is a single-arm forward spectrometer covering the pseudorapidity range $2 < \eta < 5$, designed for the study of particles containing b or c quarks. The detector includes a high-precision tracking system consisting of a silicon-strip vertex detector surrounding the pp interaction region [14], a large-area silicon-strip detector located upstream of a dipole magnet with a bending power of about 4 Tm, the polarity of which can be inverted, and three stations of silicon-strip detectors and straw drift tubes [15] placed downstream of the magnet. The tracking system provides a measurement of momentum, p , with a relative uncertainty that varies from 0.4% at low momentum to 0.6% at 100 GeV/ c . The minimum distance of a track to a primary vertex, the impact parameter, is measured with a resolution of $(15 + 29/p_T)$ μm , where p_T is the component of the momentum transverse to the beam, in GeV/ c . Different types of charged hadrons are distinguished using information from two ring-imaging Cherenkov detectors. Photon, electron and hadron candidates are identified by a calorimeter system consisting of scintillating-pad and preshower detectors, an electromagnetic calorimeter and a hadronic calorimeter. Muons are identified by a system composed of alternating layers of iron and multiwire proportional chambers. The trigger [16] consists of a hardware stage, based on information from the calorimeter and muon systems, followed by a software stage, which applies a full event reconstruction.

In the simulation, pp collisions are generated using PYTHIA 6 [2] with a specific LHCb configuration [17] using the CTEQ6 leading-order parton density functions. Decays of hadronic particles are described by EVTGEN [18], in which final-state radiation is generated using PHOTOS [19]. The interaction of the generated particles with the detector, and its response, are implemented using the GEANT4 toolkit [20,21] as described in Ref. [22].

The data used in this analysis are a subset of the data recorded during low-luminosity running in early 2010 with a minimum bias trigger where the hardware stage triggered every beam-beam crossing and the event was accepted at the software stage if at least one reconstructed track segment was found in the vertex detector. Using a sample of no-bias triggered events, it has been checked that for the events selected in this analysis, the trigger efficiency exceeds 99.99%. From the rate of empty events the average number of interactions per bunch crossing, μ , with at least one track in the detector, was estimated to be 0.1. This corresponds to $P = \mu/(1 - \exp(-\mu)) \approx 1.05$ visible interactions per triggered event. The measurement is based on integrated luminosities of 0.62 (1.25) nb^{-1} recorded with the magnetic field polarity in the upward (downward) direction. The integrated luminosity has been determined with an overall precision of 3.5% [23].

3 Data analysis

This analysis measures the inelastic pp cross-section for the production of at least one prompt long-lived charged particle with $p_T > 0.2$ GeV/ c and pseudorapidity in the range $2.0 < \eta < 4.5$. A prompt particle is defined as one whose impact parameter relative to the point of the primary interaction is smaller than 200 μm .

The LHCb coordinate system is a right-handed cartesian system with the z axis along the average beam direction from the vertex detector towards the muon system, the y axis pointing upward and x towards the outside of the LHC. Reconstructed tracks are required to have a track segment in the vertex detector and in the tracking system downstream of the magnet. Selection criteria (cuts) are applied on the track fit χ^2/NDF , with NDF the number of degrees of freedom of the fit, and on the distance of closest approach, DCA, to the longitudinal axis of the luminous region. This axis is determined by the mean values of Gaussian functions fitted in bins of z to the x and y distributions of reconstructed primary vertices. To suppress background from beam-gas interactions, the z coordinate of the midpoint between the points of closest approach on the reconstructed particle trajectory and on the longitudinal axis of the luminous region is required to satisfy $|z - z_c| < 130$ mm. Here z_c is the longitudinal centre of the luminous region, determined by the mean value of a Gaussian function fitted to the z distribution of the reconstructed primary vertices. The width of the distribution is found to be $\sigma_z = 38.2$ mm. The determination of the central axis of the luminous region and its longitudinal centre is done separately for each magnet polarity. The analysis is restricted to tracks in a fiducial region away from areas where the magnetic field or detector geometry cause sharp variations in the track finding efficiency.

The cross-section, $\sigma_{\text{inel}}^{\text{acc}}$, for inelastic pp collisions yielding one or more prompt long-lived charged particles in the kinematic range $p_T > 0.2$ GeV/ c and $2.0 < \eta < 4.5$ is obtained using the expression

$$\sigma_{\text{inel}}^{\text{acc}} = \frac{I^{\text{acc}}}{L} = \frac{N^{\text{vis}}}{\varepsilon \cdot L}. \quad (1)$$

Here I^{acc} is the number of pp interactions in data with a least one prompt charged par-

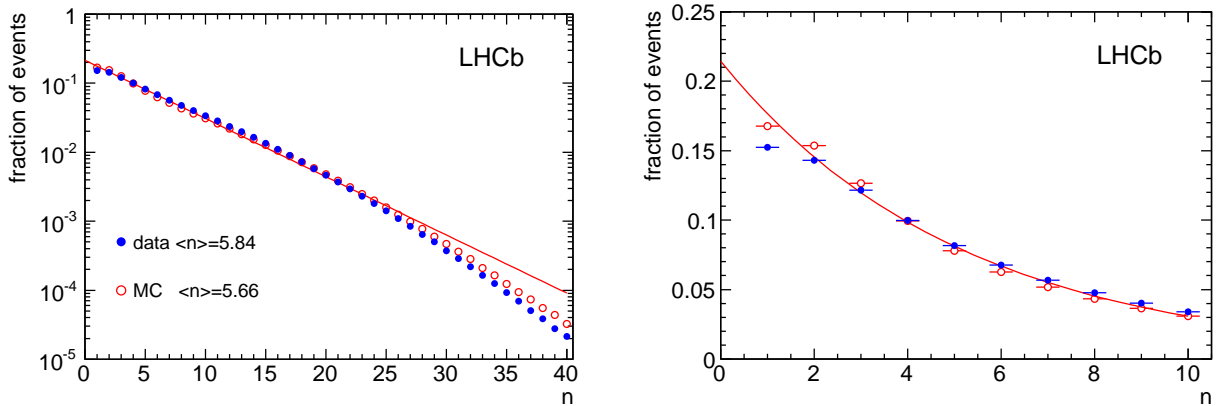


Figure 1: Normalized track multiplicity distributions with $n \geq 1$ tracks in the fiducial region for the field-down configuration and tight cut settings in data and simulation. The superimposed function is an exponential with the same average as the simulation. The right hand plot with a linear scale shows a zoom of the low-multiplicity region. The vertical error bars are smaller than the symbol sizes.

ticle in the kinematic acceptance $p_T > 0.2 \text{ GeV}/c$ and $2.0 < \eta < 4.5$ while L is the integrated luminosity of the data set under consideration. The number of interactions I^{acc} is proportional to the experimentally observed number of events, N^{vis} , with at least one reconstructed track in the fiducial region. The ratio $\varepsilon = N^{\text{vis}}/I^{\text{acc}}$ is determined from the full simulation, which includes the possibility of multiple interactions per event,

$$\varepsilon = \frac{N_{\text{MC}}^{\text{vis}}}{I_{\text{MC}}^{\text{acc}}} = \frac{N_{\text{MC}}^{\text{vis}}}{I_{\text{MC}}^{\text{vis}}} \cdot \frac{I_{\text{MC}}^{\text{vis}}}{I_{\text{MC}}^{\text{acc}}}. \quad (2)$$

The first factor, the ratio $N_{\text{MC}}^{\text{vis}}/I_{\text{MC}}^{\text{vis}}$ of events and interactions with at least one reconstructed track in the fiducial region, corrects for the fraction of multiple interactions. The second factor, the ratio $I_{\text{MC}}^{\text{vis}}/I_{\text{MC}}^{\text{acc}}$, is the efficiency to detect a single interaction with at least one prompt electron, muon, pion, kaon, proton or the corresponding antiparticle, in the kinematic acceptance.

To study the sensitivity of the analysis to the choice of the cuts on track quality and DCA, the measurements are performed for two cases: “loose” settings accepting most reconstructed tracks, and “tight” ones selecting mainly the cores of the χ^2/NDF and DCA distributions.

Figure 1 shows the normalized multiplicity distributions of tracks from the luminous region that are recorded in the fiducial region of the analysis for the tight cut settings in the field-down configuration. The distributions have an approximately exponential shape, as can be seen from the superimposed curves. The small disagreement seen at low multiplicities is addressed when discussing systematic uncertainties.

Table 1 gives the interaction and event counts in simulation and data. The simulations are based on a total of I_{MC} inelastic pp interactions. The event counts in the simulation are given for an average of $P = 1.05$ interactions per event and for both settings of the analysis cuts. One finds a typical value for the correction factor ε of 0.87. For a

Table 1: Numbers of interactions and events, in multiples of 10^6 , in simulation and data for different magnetic field configurations and analysis cuts, and the resulting cross-sections in the kinematic acceptance.

Simulation	field-down	field-up
I_{MC}	31.784	4.948
$I_{\text{MC}}^{\text{acc}}$	26.121	4.067
$N_{\text{MC}}^{\text{vis}}$ (loose cuts)	22.907	3.584
$N_{\text{MC}}^{\text{vis}}$ (tight cuts)	22.693	3.551
Data		
N^{vis} (loose cuts)	30.098	60.285
N^{vis} (tight cuts)	29.735	59.541
Cross-section [mb]		
$\sigma_{\text{inel}}^{\text{acc}}$ (loose cuts)	55.36	54.73
$\sigma_{\text{inel}}^{\text{acc}}$ (tight cuts)	55.20	54.55

given magnet polarity, the inelastic cross-section is taken to be the central value of the measurements with loose and tight cuts. The final cross-section result is determined by the arithmetic average of the central values for the two magnet polarities. Here any biases that change sign under inversion of the field cancel exactly and uncertainties that are not fully correlated between the two configurations are reduced. Within the acceptance of LHCb, the inelastic pp cross-section with at least one prompt long-lived charged particle having $p_{\text{T}} > 0.2 \text{ GeV}/c$ and $2.0 < \eta < 4.5$ is found to be $\sigma_{\text{inel}}^{\text{acc}} = 54.96 \pm 0.01 \text{ mb}$, where the uncertainty is purely statistical.

4 Systematic uncertainties

The systematic uncertainties are determined separately for the two magnet settings and are combined taking into account the correlations between the individual contributions. The dominant uncertainty comes from the integrated luminosity, which is known with a precision of 3.5%. The sensitivity to the knowledge of the fraction of multiple interactions was tested by varying P in the simulation in the range $1.025 \leq P \leq 1.075$, which leads to a variation in the cross-section of 1.5%.

Several systematic effects are related to a possible mismatch in the distributions of the selection variables between data and simulation. The determination of the impact of the selection cuts on the event selection efficiency requires a proper modelling of the tails of the distributions of the selection variables. The corresponding systematic uncertainties are found to be 0.3% by varying the selection cuts between loose and tight settings. The influence of the detector calibration on the reconstruction of charged tracks is tested by comparing the nominal event counts with those obtained when using an alternative version of the reconstruction code. For the loose cuts the changes are small, but for the

Table 2: Summary of the relative systematic uncertainties, expressed as a percentage, for the measurement of the inelastic pp cross-section measurement, separately for the two magnet polarities and the combined value.

Source	field-down	field-up	combined
Luminosity	3.5	3.5	3.5
Multiple interactions	1.5	1.5	1.5
Selection cuts	0.3	0.3	0.3
Calibration	1.1	0.5	0.8
Track finding efficiency	0.8	0.8	0.8
Charged particle multiplicities	1.0	1.0	1.0
Data taking period	1.0	1.0	0.7
Azimuthal dependence	1.3	1.3	0.9
Magnet polarity	0.6	0.6	0.6

tight cuts variations in the event counts of 1.1% for field-down and 0.5% for field-up are observed, which are assigned as systematic uncertainties. The systematic uncertainty on the reconstruction efficiency of a single track was found to be 3% [24]. After convolution with the track multiplicity distribution of the events, this translates into an uncertainty of 0.8% in the event selection efficiency. The systematic uncertainty related to the modelling of the charged particle multiplicity distribution in the kinematic acceptance is estimated from the difference between the observed average multiplicities in data and simulation. At generator level the difference is about twice as large, and a systematic uncertainty of 0.5 units is assigned, which translates to a 1% uncertainty in the event selection efficiency.

The cross-section measurement has been performed as a function of data taking period and in different azimuthal regions. Small but statistically significant variations are observed in both cases. From the maximum variations seen, uncertainties of 1.0% and 1.3% are assigned for dependencies on data taking period and azimuthal region, respectively. Finally, comparing the cross-section measurements for the field polarities one observes a difference of about 1.2%. Half of that variation is assigned as a systematic uncertainty.

The analysis has been performed in the LHCb laboratory frame which, due to a small crossing angle between the LHC beams, is slightly boosted with respect to the pp centre-of-mass system. It has been checked using simulation that this small boost has an impact of less than 0.1% on the cross-section measurement. The contamination from elastic scattering events has been estimated to be negligible, and the statistical uncertainty due to the finite size of the Monte Carlo sample is less than 0.1% and is neglected. Table 2 gives a summary of the systematic uncertainties. For the combination of the two magnet polarities, the dependence on data taking period and the azimuthal dependence are assumed to be uncorrelated, while the other uncertainties are assumed to be fully correlated. Adding the combined contributions in quadrature, the total systematic uncertainty on the cross-section is 4.3%.

5 Results

The cross-section for inelastic pp collisions at a centre-of-mass energy $\sqrt{s} = 7$ TeV, yielding one or more prompt long-lived charged particles in the kinematic range $p_T > 0.2$ GeV/ c and $2.0 < \eta < 4.5$, is

$$\sigma_{\text{inel}}^{\text{acc}}(p_T > 0.2 \text{ GeV}/c, 2.0 < \eta < 4.5) = 55.0 \pm 2.4 \text{ mb} ,$$

with an uncertainty that is almost completely systematic in nature. The purely statistical uncertainty is two orders of magnitude smaller.

The measurement within the limited kinematic range above is scaled to full phase space with an extrapolation factor, s_{extr} , which is given by the ratio of all inelastic interactions to the number of inelastic interactions within the kinematic acceptance. The PYTHIA 6 simulation used in the efficiency determination [2, 17] gives $s_{\text{extr}} = I_{\text{MC}}/I_{\text{MC}}^{\text{acc}} = 1.2168 \pm 0.0001$, where the uncertainty is statistical.

The extrapolation to full phase space is necessarily model dependent. To estimate its uncertainty, different soft QCD tunes provided by PYTHIA 8.201 (see Ref. [25] and references therein) have been considered: **4Cx**, a tune derived from the **2C**-tune to CDF data and adapted to LHC; **Monash 2013**, a tune based on both e^+e^- and LHC data; **A2-CTEQ6L1**, **A2-MSTW2008LO**, **AU2-CTEQ6L1** and **AU2-MSTW2008LO**, minimum bias and underlying event tunes by the ATLAS collaboration using the CTEQ 6L1 and the MSTW2008 LO parton densities; and **CUETP8S1-CTEQ6L1**, an underlying event tune by the CMS collaboration. Table 3 summarizes some average properties of those tunes for non-diffractive, single-diffractive and double-diffractive interactions. Mean values and standard deviations are given for n , the zero-suppressed average multiplicity of prompt long-lived charged particles in the kinematic acceptance, for the visibility v , defined by the probability that at least one charged particle is inside the kinematic acceptance, and for the fraction f of each interaction type. For any mix of interaction types, extrapolation factor and visibility are related by $s_{\text{extr}} = 1/v$.

The extrapolation factor, converting the inelastic cross-section in the kinematic acceptance to the total inelastic cross-section, is a function of the visibilities and the fractions of non-diffractive, single-diffractive and double-diffractive interactions. Since the interaction-type fractions are only weakly constrained by experiment (see e.g. Ref. [7]), the values of f given in Table 3 are not used in the following. To determine an estimate for the uncertainty of the extrapolation factor, a Monte Carlo approach is used. Multiplicities and visibilities are generated according to Gaussian densities with parameters as given in Table 3. The interaction type fractions that go into the extrapolation factor are then determined subject to the constraints that each of them lies between zero and one, that they sum to unity, and that the zero-suppressed average multiplicity of the mix is consistent with the generator level average multiplicity of the PYTHIA 6 simulation, 10.93, which provides a good description of the data. The distribution of the average multiplicity is modelled according to a Gaussian function with this mean value and standard deviation 0.5.

The method yields a distribution for s_{extr} with an average of 1.17 and a standard devi-

Table 3: Properties of soft QCD tunes in PYTHIA 8.201. For non-diffractive, single-diffractive and double-diffractive interactions, mean value and standard deviation over the tunes considered in this study are given for average multiplicities inside the kinematic acceptance, visibilities and interaction type fractions.

interaction type	n	v	f
non-diffractive	12.22 ± 0.50	0.9925 ± 0.0003	0.713 ± 0.002
single-diffractive	5.94 ± 0.29	0.5059 ± 0.0049	0.173 ± 0.002
double-diffractive	4.78 ± 0.17	0.5819 ± 0.0062	0.114 ± 0.001

ation of 0.08, which is assigned as the systematic uncertainty on the extrapolation factor obtained from the fully simulated Monte Carlo. The event fractions found by the above procedure, 0.70 ± 0.12 , 0.17 ± 0.06 and 0.13 ± 0.05 for non-diffractive, single-diffractive and double-diffractive interactions, respectively, are consistent with the fractions given by the various tunes. The total inelastic cross-section becomes

$$\sigma_{\text{inel}} = 66.9 \pm 2.9 (\text{exp}) \pm 4.4 (\text{extr}) \text{ mb} ,$$

with an experimental uncertainty (exp) that is dominated by systematic contributions and an extrapolation uncertainty (extr) of 7%.

The LHCb result is displayed together with other cross-section measurements at various energies in Fig. 2. The data for the total cross-section are taken from Ref. [26] and for the inelastic cross-section from Ref. [27]. The plot shows that the available measurements at centre-of-mass energies $\sqrt{s} > 100$ GeV can be described by a power-law behaviour. A $\ln^2 s$ behaviour, as asymptotically expected if the Froissart-Martin bound is saturated, is not observed within the current experimental uncertainties. For comparison, results by the other LHC experiments are also shown. The TOTEM [11, 12] and the ATLAS [9] results are based on a measurement of the elastic cross-section, neither of which requires an extrapolation from a limited angular acceptance to full phase space. Within the extrapolation uncertainties all results are in good agreement. Nevertheless, to avoid introducing ambiguities due to the model dependence of the extrapolation, any comparison between theory and the measurement presented in this paper should be done for the restricted kinematic range $p_T > 0.2$ GeV/ c and $2.0 < \eta < 4.5$.

Acknowledgements

We express our gratitude to our colleagues in the CERN accelerator departments for the excellent performance of the LHC. We thank the technical and administrative staff at the LHCb institutes. We acknowledge support from CERN and from the national agencies: CAPES, CNPq, FAPERJ and FINEP (Brazil); NSFC (China); CNRS/IN2P3 (France); BMBF, DFG, HGF and MPG (Germany); INFN (Italy); FOM and NWO (The Netherlands); MNiSW and NCN (Poland); MEN/IFA (Romania); MinES and FANO (Russia); MinECo (Spain); SNSF and SER (Switzerland); NASU (Ukraine); STFC (United

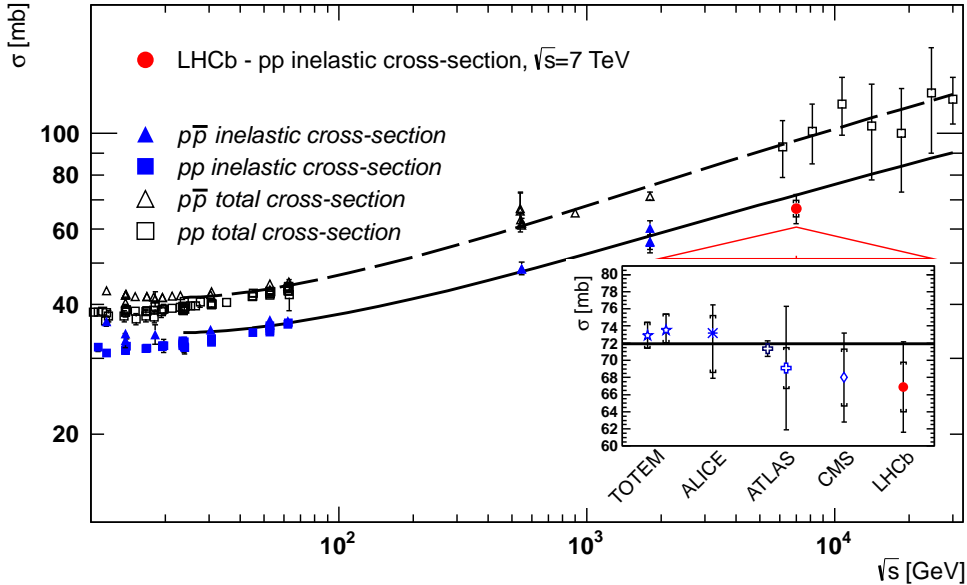


Figure 2: Inelastic cross-section measured by LHCb compared to the existing data on the total [26] and inelastic cross-sections [27] in pp and $p\bar{p}$ collisions as a function to the centre-of-mass energy. The full (dashed) line is a phenomenological fit [28] of the energy dependence of the inelastic (total) cross-section. The main plot only shows the LHCb measurement. The inset is a zoom, comparing all inelastic cross-section measurements by the LHC experiments ALICE [7], ATLAS [8, 9], CMS [10] and TOTEM [11, 12]. The horizontal line represents the value of the phenomenological fit at $\sqrt{s} = 7$ TeV. The error bars give the total uncertainties of the measurements. When an inner error bar is shown, it represents the experimental uncertainties added in quadrature, while the full error bar also covers an extrapolation uncertainty.

Kingdom); NSF (USA). The Tier1 computing centres are supported by IN2P3 (France), KIT and BMBF (Germany), INFN (Italy), NWO and SURF (The Netherlands), PIC (Spain), GridPP (United Kingdom). We are indebted to the communities behind the multiple open source software packages on which we depend. We are also thankful for the computing resources and the access to software R&D tools provided by Yandex LLC (Russia). Individual groups or members have received support from EPLANET, Marie Skłodowska-Curie Actions and ERC (European Union), Conseil général de Haute-Savoie, Labex ENIGMASS and OCEVU, Région Auvergne (France), RFBR (Russia), XuntaGal and GENCAT (Spain), Royal Society and Royal Commission for the Exhibition of 1851 (United Kingdom).

References

- [1] J. Knapp, *High-energy interactions and extensive air showers*, [arXiv:astro-ph/9710277](#).
- [2] T. Sjöstrand, S. Mrenna, and P. Skands, *PYTHIA 6.4 Physics and manual*, JHEP **05** (2006) 026, [arXiv:hep-ph/0603175](#).
- [3] T. Sjöstrand, S. Mrenna, and P. Skands, *A brief introduction to PYTHIA 8.1*, Comput. Phys. Commun. **178** (2008) 852, [arXiv:0710.3820](#).
- [4] M. Froissart, *Asymptotic behavior and subtractions in the Mandelstam representation.*, Phys. Rev. **123** (1961) 1053.
- [5] A. Martin, *Extension of the axiomatic analyticity domain of scattering amplitudes by unitarity - I.*, Nuovo Cimento **42A** (1966) 930.
- [6] A. Martin, *Froissart bound for inelastic cross sections*, Phys. Rev. **D80** (2009) 065013, [arXiv:0904.3724](#).
- [7] ALICE collaboration, B. Abelev *et al.*, *Measurement of inelastic, single- and double-diffraction cross sections in proton–proton collisions at the LHC with ALICE*, Eur. Phys. J. **C73** (2013) 2456, [arXiv:1208.4968](#).
- [8] ATLAS collaboration, G. Aad *et al.*, *Measurement of the inelastic proton-proton cross-section at $\sqrt{s} = 7$ TeV with the ATLAS detector*, Nature Communications **2** (2011) 463, [arXiv:1104.0326](#).
- [9] ATLAS collaboration, G. Aad *et al.*, *Measurement of the total cross-section from elastic scattering in pp collisions at $\sqrt{s} = 7$ TeV with the ATLAS detector*, Nucl. Phys. **B889** (2014) 486, [arXiv:1408.5778](#).
- [10] CMS collaboration, S. Chatrchyan *et al.*, *Measurement of the inelastic pp cross section at $\sqrt{s} = 7$ TeV with the CMS detector*, Phys. Lett. **B722** (2013) 5, [arXiv:1210.6718](#).
- [11] TOTEM collaboration, G. Antchev *et al.*, *First measurement of the total proton-proton cross section at the LHC energy of $\sqrt{s} = 7$ TeV*, Europhys. Lett. **96** (2011) 21002, [arXiv:1110.1395](#).
- [12] TOTEM, G. Antchev *et al.*, *Luminosity-independent measurements of total, elastic and inelastic cross-sections at $\sqrt{s} = 7$ TeV*, Europhys. Lett. **101** (2013) 21004.
- [13] LHCb collaboration, A. A. Alves Jr. *et al.*, *The LHCb detector at the LHC*, JINST **3** (2008) S08005.
- [14] R. Aaij *et al.*, *Performance of the LHCb Vertex Locator*, JINST **9** (2014) 09007, [arXiv:1405.7808](#).

- [15] R. Arink *et al.*, *Performance of the LHCb Outer Tracker*, JINST **9** (2014) P01002, [arXiv:1311.3893](#).
- [16] R. Aaij *et al.*, *The LHCb trigger and its performance in 2011*, JINST **8** (2013) P04022, [arXiv:1211.3055](#).
- [17] I. Belyaev *et al.*, *Handling of the generation of primary events in Gauss, the LHCb simulation framework*, Nuclear Science Symposium Conference Record (NSS/MIC) **IEEE** (2010) 1155.
- [18] D. J. Lange, *The EVTGEN particle decay simulation package*, Nucl. Instrum. Meth. **A462** (2001) 152.
- [19] P. Golonka and Z. Was, *PHOTOS Monte Carlo: A precision tool for QED corrections in Z and W decays*, Eur. Phys. J. **C45** (2006) 97, [arXiv:hep-ph/0506026](#).
- [20] GEANT4 collaboration, J. Allison *et al.*, *GEANT4 developments and applications*, IEEE Trans. Nucl. Sci. **53** (2006) 270.
- [21] GEANT4 collaboration, S. Agostinelli *et al.*, *GEANT4: A simulation toolkit*, Nucl. Instrum. Meth. **A506** (2003) 250.
- [22] M. Clemencic *et al.*, *The LHCb simulation application, GAUSS: design, evolution and experience*, J. of Phys: Conf. Ser. **331** (2011) 032023.
- [23] LHCb collaboration, R. Aaij *et al.*, *Absolute luminosity measurements with the LHCb detector at the LHC*, JINST **7** (2012) P01010, [arXiv:1110.2866](#).
- [24] LHCb collaboration, R. Aaij *et al.*, *Measurement of $\sigma(pp \rightarrow b\bar{b}X)$ at $\sqrt{s} = 7$ TeV in the forward region*, Phys. Lett. **B694** (2010) 209, [arXiv:1009.2731](#).
- [25] T. Sjöstrand *et al.*, *A brief introduction to PYTHIA 8.2*, [arXiv:1410.3012](#).
- [26] Particle Data Group, K. Olive *et al.*, *Review of particle physics*, Chin. Phys. **C38** (2014) 090001.
- [27] A. Achilli *et al.*, *Total and inelastic cross-sections at LHC at $\sqrt{s} = 7$ TeV and beyond*, Phys. Rev. **D84** (2011) 094009, [arXiv:1102.1949](#).
- [28] D. A. Fagundes, M. J. Menon, and P. V. R. G. Silva, *On the rise of proton-proton cross-sections at high energies*, J. Phys. **G40** (2013) 065005, [arXiv:1208.3456](#).

LHCb collaboration

R. Aaij⁴¹, B. Adeva³⁷, M. Adinolfi⁴⁶, A. Affolder⁵², Z. Ajaltouni⁵, S. Akar⁶, J. Albrecht⁹, F. Alessio³⁸, M. Alexander⁵¹, S. Ali⁴¹, G. Alkhazov³⁰, P. Alvarez Cartelle³⁷, A.A. Alves Jr^{25,38}, S. Amato², S. Amerio²², Y. Amhis⁷, L. An³, L. Anderlini^{17,g}, J. Anderson⁴⁰, R. Andreassen⁵⁷, M. Andreotti^{16,f}, J.E. Andrews⁵⁸, R.B. Appleby⁵⁴, O. Aquines Gutierrez¹⁰, F. Archilli³⁸, A. Artamonov³⁵, M. Artuso⁵⁹, E. Aslanides⁶, G. Auriemma^{25,n}, M. Baalouch⁵, S. Bachmann¹¹, J.J. Back⁴⁸, A. Badalov³⁶, C. Baesso⁶⁰, W. Baldini¹⁶, R.J. Barlow⁵⁴, C. Barschel³⁸, S. Barsuk⁷, W. Barter⁴⁷, V. Batozskaya²⁸, V. Battista³⁹, A. Bay³⁹, L. Beaucourt⁴, J. Beddow⁵¹, F. Bedeschi²³, I. Bediaga¹, S. Belogurov³¹, K. Belous³⁵, I. Belyaev³¹, E. Ben-Haim⁸, G. Bencivenni¹⁸, S. Benson³⁸, J. Benton⁴⁶, A. Berezhnoy³², R. Bernet⁴⁰, A. Bertolin²², M.-O. Bettler⁴⁷, M. van Beuzekom⁴¹, A. Bien¹¹, S. Bifani⁴⁵, T. Bird⁵⁴, A. Bizzeti^{17,i}, P.M. Bjørnstad⁵⁴, T. Blake⁴⁸, F. Blanc³⁹, J. Blouw¹⁰, S. Blusk⁵⁹, V. Bocci²⁵, A. Bondar³⁴, N. Bondar^{30,38}, W. Bonivento¹⁵, S. Borghi⁵⁴, A. Borgia⁵⁹, M. Borsato⁷, T.J.V. Bowcock⁵², E. Bowen⁴⁰, C. Bozzi¹⁶, D. Brett⁵⁴, M. Britsch¹⁰, T. Britton⁵⁹, J. Brodzicka⁵⁴, N.H. Brook⁴⁶, H. Brown⁵², A. Bursche⁴⁰, J. Buytaert³⁸, S. Cadeddu¹⁵, R. Calabrese^{16,f}, M. Calvi^{20,k}, M. Calvo Gomez^{36,p}, P. Campana¹⁸, D. Campora Perez³⁸, A. Carbone^{14,d}, G. Carboni^{24,l}, R. Cardinale^{19,38,j}, A. Cardini¹⁵, L. Carson⁵⁰, K. Carvalho Akiba^{2,38}, RCM Casanova Mohr³⁶, G. Casse⁵², L. Cassina^{20,k}, L. Castillo Garcia³⁸, M. Cattaneo³⁸, Ch. Cauet⁹, R. Cenci^{23,t}, M. Charles⁸, Ph. Charpentier³⁸, M. Chefdeville⁴, S. Chen⁵⁴, S.-F. Cheung⁵⁵, N. Chiapolini⁴⁰, M. Chrzasczcz^{40,26}, X. Cid Vidal³⁸, G. Ciezarek⁴¹, P.E.L. Clarke⁵⁰, M. Clemencic³⁸, H.V. Cliff⁴⁷, J. Closier³⁸, V. Coco³⁸, J. Cogan⁶, E. Cogneras⁵, V. Cogoni¹⁵, L. Cojocariu²⁹, G. Collazuol²², P. Collins³⁸, A. Comerma-Montells¹¹, A. Contu^{15,38}, A. Cook⁴⁶, M. Coombes⁴⁶, S. Coquereau⁸, G. Corti³⁸, M. Corvo^{16,f}, I. Counts⁵⁶, B. Couturier³⁸, G.A. Cowan⁵⁰, D.C. Craik⁴⁸, A.C. Crocombe⁴⁸, M. Cruz Torres⁶⁰, S. Cunliffe⁵³, R. Currie⁵³, C. D'Ambrosio³⁸, J. Dalseno⁴⁶, P. David⁸, P.N.Y. David⁴¹, A. Davis⁵⁷, K. De Bruyn⁴¹, S. De Capua⁵⁴, M. De Cian¹¹, J.M. De Miranda¹, L. De Paula², W. De Silva⁵⁷, P. De Simone¹⁸, C.-T. Dean⁵¹, D. Decamp⁴, M. Deckenhoff⁹, L. Del Buono⁸, N. Déléage⁴, D. Derkach⁵⁵, O. Deschamps⁵, F. Dettori³⁸, A. Di Canto³⁸, H. Dijkstra³⁸, S. Donleavy⁵², F. Dordei¹¹, M. Dorigo³⁹, A. Dosil Suárez³⁷, D. Dossett⁴⁸, A. Dovbnya⁴³, K. Dreimanis⁵², G. Dujany⁵⁴, F. Dupertuis³⁹, P. Durante³⁸, R. Dzhelyadin³⁵, A. Dziurda²⁶, A. Dzyuba³⁰, S. Easo^{49,38}, U. Egede⁵³, V. Egorychev³¹, S. Eidelman³⁴, S. Eisenhardt⁵⁰, U. Eitschberger⁹, R. Ekelhof⁹, L. Eklund⁵¹, I. El Rifai⁵, Ch. Elsasser⁴⁰, S. Ely⁵⁹, S. Esen¹¹, H.M. Evans⁴⁷, T. Evans⁵⁵, A. Falabella¹⁴, C. Färber¹¹, C. Farinelli⁴¹, N. Farley⁴⁵, S. Farry⁵², R. Fay⁵², D. Ferguson⁵⁰, V. Fernandez Albor³⁷, F. Ferreira Rodrigues¹, M. Ferro-Luzzi³⁸, S. Filippov³³, M. Fiore^{16,f}, M. Fiorini^{16,f}, M. Firlej²⁷, C. Fitzpatrick³⁹, T. Fiutowski²⁷, P. Fol⁵³, M. Fontana¹⁰, F. Fontanelli^{19,j}, R. Forty³⁸, O. Francisco², M. Frank³⁸, C. Frei³⁸, M. Frosini¹⁷, J. Fu^{21,38}, E. Furfaro^{24,l}, A. Gallas Torreira³⁷, D. Galli^{14,d}, S. Gallorini^{22,38}, S. Gambetta^{19,j}, M. Gandelman², P. Gandini⁵⁹, Y. Gao³, J. García Pardiñas³⁷, J. Garofoli⁵⁹, J. Garra Tico⁴⁷, L. Garrido³⁶, D. Gascon³⁶, C. Gaspar³⁸, U. Gastaldi¹⁶, R. Gauld⁵⁵, L. Gavardi⁹, A. Geraci^{21,v}, E. Gersabeck¹¹, M. Gersabeck⁵⁴, T. Gershon⁴⁸, Ph. Ghez⁴, A. Gianelle²², S. Giani³⁹, V. Gibson⁴⁷, L. Giubega²⁹, V.V. Gligorov³⁸, C. Göbel⁶⁰, D. Golubkov³¹, A. Golutvin^{53,31,38}, A. Gomes^{1,a}, C. Gotti^{20,k}, M. Grabalosa Gándara⁵, R. Graciani Diaz³⁶, L.A. Granado Cardoso³⁸, E. Graugés³⁶, E. Graverini⁴⁰, G. Graziani¹⁷, A. Grecu²⁹, E. Greening⁵⁵, S. Gregson⁴⁷, P. Griffith⁴⁵, L. Grillo¹¹, O. Grünberg⁶³, B. Gui⁵⁹, E. Gushchin³³, Yu. Guz^{35,38}, T. Gys³⁸, C. Hadjivasiliou⁵⁹, G. Haefeli³⁹, C. Haen³⁸, S.C. Haines⁴⁷, S. Hall⁵³,

B. Hamilton⁵⁸, T. Hampson⁴⁶, X. Han¹¹, S. Hansmann-Menzemer¹¹, N. Harnew⁵⁵,
 S.T. Harnew⁴⁶, J. Harrison⁵⁴, J. He³⁸, T. Head³⁹, V. Heijne⁴¹, K. Hennessy⁵², P. Henrard⁵,
 L. Henry⁸, J.A. Hernando Morata³⁷, E. van Herwijnen³⁸, M. Heß⁶³, A. Hicheur², D. Hill⁵⁵,
 M. Hoballah⁵, C. Hombach⁵⁴, W. Hulsbergen⁴¹, N. Hussain⁵⁵, D. Hutchcroft⁵², D. Hynds⁵¹,
 M. Idzik²⁷, P. Ilten⁵⁶, R. Jacobsson³⁸, A. Jaeger¹¹, J. Jalocho⁵⁵, E. Jans⁴¹, P. Jatón³⁹,
 A. Jawahery⁵⁸, F. Jing³, M. John⁵⁵, D. Johnson³⁸, C.R. Jones⁴⁷, C. Joram³⁸, B. Jost³⁸,
 N. Jurik⁵⁹, S. Kandybei⁴³, W. Kanso⁶, M. Karacson³⁸, T.M. Karbach³⁸, S. Karodia⁵¹,
 M. Kelsey⁵⁹, I.R. Kenyon⁴⁵, T. Ketel⁴², B. Khanji^{20,38,k}, C. Khurewathanakul³⁹, S. Klaver⁵⁴,
 K. Klimaszewski²⁸, O. Kochebina⁷, M. Kolpin¹¹, I. Komarov³⁹, R.F. Koopman⁴²,
 P. Koppenburg^{41,38}, M. Korolev³², L. Kravchuk³³, K. Kreplin¹¹, M. Kreps⁴⁸, G. Krocker¹¹,
 P. Krokovny³⁴, F. Kruse⁹, W. Kucewicz^{26,o}, M. Kucharczyk^{20,26,k}, V. Kudryavtsev³⁴,
 K. Kurek²⁸, T. Kvaratskheliya³¹, V.N. La Thi³⁹, D. Lacarrere³⁸, G. Lafferty⁵⁴, A. Lai¹⁵,
 D. Lambert⁵⁰, R.W. Lambert⁴², G. Lanfranchi¹⁸, C. Langenbruch⁴⁸, B. Langhans³⁸,
 T. Latham⁴⁸, C. Lazzeroni⁴⁵, R. Le Gac⁶, J. van Leerdam⁴¹, J.-P. Lees⁴, R. Lefèvre⁵,
 A. Leflat³², J. Lefrançois⁷, S. Leo²³, O. Leroy⁶, T. Lesiak²⁶, B. Leverington¹¹, Y. Li³,
 T. Likhomanenko⁶⁴, M. Liles⁵², R. Lindner³⁸, C. Linn³⁸, F. Lionetto⁴⁰, B. Liu¹⁵, S. Lohn³⁸,
 I. Longstaff⁵¹, J.H. Lopes², P. Lowdon⁴⁰, D. Lucchesi^{22,r}, H. Luo⁵⁰, A. Lupato²², E. Luppi^{16,f},
 O. Lupton⁵⁵, F. Machefert⁷, I.V. Machikhiliyan³¹, F. Maciuc²⁹, O. Maev³⁰, S. Malde⁵⁵,
 A. Malinin⁶⁴, G. Manca^{15,e}, G. Mancinelli⁶, A. Mapelli³⁸, J. Maratas⁵, J.F. Marchand⁴,
 U. Marconi¹⁴, C. Marin Benito³⁶, P. Marino^{23,t}, R. Märki³⁹, J. Marks¹¹, G. Martellotti²⁵,
 A. Martín Sánchez⁷, M. Martinelli³⁹, D. Martinez Santos^{42,38}, F. Martinez Vidal⁶⁵,
 D. Martins Tostes², A. Massafferri¹, R. Matev³⁸, Z. Mathe³⁸, C. Matteuzzi²⁰, A. Mazurov⁴⁵,
 M. McCann⁵³, J. McCarthy⁴⁵, A. McNab⁵⁴, R. McNulty¹², B. McSkelly⁵², B. Meadows⁵⁷,
 F. Meier⁹, M. Meissner¹¹, M. Merk⁴¹, D.A. Milanes⁶², M.-N. Minard⁴, N. Moggi¹⁴,
 J. Molina Rodriguez⁶⁰, S. Monteil⁵, M. Morandin²², P. Morawski²⁷, A. Mordà⁶,
 M.J. Morello^{23,t}, J. Moron²⁷, A.-B. Morris⁵⁰, R. Mountain⁵⁹, F. Muheim⁵⁰, K. Müller⁴⁰,
 M. Mussini¹⁴, B. Muster³⁹, P. Naik⁴⁶, T. Nakada³⁹, R. Nandakumar⁴⁹, I. Nasteva²,
 M. Needham⁵⁰, N. Neri²¹, S. Neubert³⁸, N. Neufeld³⁸, M. Neuner¹¹, A.D. Nguyen³⁹,
 T.D. Nguyen³⁹, C. Nguyen-Mau^{39,q}, M. Nicol⁷, V. Niess⁵, R. Niet⁹, N. Nikitin³²,
 T. Nikodem¹¹, A. Novoselov³⁵, D.P. O’Hanlon⁴⁸, A. Oblakowska-Mucha^{27,38}, V. Obraztsov³⁵,
 S. Oggero⁴¹, S. Ogilvy⁵¹, O. Okhrimenko⁴⁴, R. Oldeman^{15,e}, C.J.G. Onderwater⁶⁶,
 M. Orlandea²⁹, J.M. Otalora Goicochea², A. Otto³⁸, P. Owen⁵³, A. Oyanguren⁶⁵, B.K. Pal⁵⁹,
 A. Palano^{13,c}, F. Palombo^{21,u}, M. Palutan¹⁸, J. Panman³⁸, A. Papanestis^{49,38},
 M. Pappagallo⁵¹, L.L. Pappalardo^{16,f}, C. Parkes⁵⁴, C.J. Parkinson^{9,45}, G. Passaleva¹⁷,
 G.D. Patel⁵², M. Patel⁵³, C. Patrignani^{19,j}, A. Pearce^{54,49}, A. Pellegrino⁴¹, G. Penso^{25,m},
 M. Pepe Altarelli³⁸, S. Perazzini^{14,d}, P. Perret⁵, M. Perrin-Terrin⁶, L. Pescatore⁴⁵, E. Pesen⁶⁷,
 K. Petridis⁵³, A. Petrolini^{19,j}, E. Picatoste Olloqui³⁶, B. Pietrzyk⁴, T. Pilař⁴⁸, D. Pinci²⁵,
 A. Pistone¹⁹, S. Playfer⁵⁰, M. Plo Casasus³⁷, F. Polci⁸, A. Poluektov^{48,34}, I. Polyakov³¹,
 E. Polcarpo², A. Popov³⁵, D. Popov¹⁰, B. Popovici²⁹, C. Potterat², E. Price⁴⁶, J.D. Price⁵²,
 J. Prisciandaro³⁹, A. Pritchard⁵², C. Prouve⁴⁶, V. Pugatch⁴⁴, A. Puig Navarro³⁹, G. Punzi^{23,s},
 W. Qian⁴, B. Rachwal²⁶, J.H. Rademacker⁴⁶, B. Rakotomiaramanana³⁹, M. Rama¹⁸,
 M.S. Rangel², I. Raniuk⁴³, N. Rauschmayr³⁸, G. Raven⁴², F. Redi⁵³, S. Reichert⁵⁴,
 M.M. Reid⁴⁸, A.C. dos Reis¹, S. Ricciardi⁴⁹, S. Richards⁴⁶, M. Rihl³⁸, K. Rinnert⁵²,
 V. Rives Molina³⁶, P. Robbe⁷, A.B. Rodrigues¹, E. Rodrigues⁵⁴, P. Rodriguez Perez⁵⁴,
 S. Roiser³⁸, V. Romanovsky³⁵, A. Romero Vidal³⁷, M. Rotondo²², J. Rouvinet³⁹, T. Ruf³⁸,
 H. Ruiz³⁶, P. Ruiz Valls⁶⁵, J.J. Saborido Silva³⁷, N. Sagidova³⁰, P. Sail⁵¹, B. Saitta^{15,e},

V. Salustino Guimaraes², C. Sanchez Mayordomo⁶⁵, B. Sanmartin Sedes³⁷, R. Santacesaria²⁵, C. Santamarina Rios³⁷, E. Santovetti^{24,l}, A. Sarti^{18,m}, C. Satriano^{25,n}, A. Satta²⁴, D.M. Saunders⁴⁶, D. Savrina^{31,32}, M. Schiller³⁸, H. Schindler³⁸, M. Schlupp⁹, M. Schmelling¹⁰, B. Schmidt³⁸, O. Schneider³⁹, A. Schopper³⁸, M.-H. Schune⁷, R. Schwemmer³⁸, B. Sciascia¹⁸, A. Sciubba^{25,m}, A. Semennikov³¹, I. Sepp⁵³, N. Serra⁴⁰, J. Serrano⁶, L. Sestini²², P. Seyfert¹¹, M. Shapkin³⁵, I. Shapoval^{16,43,f}, Y. Shcheglov³⁰, T. Shears⁵², L. Shekhtman³⁴, V. Shevchenko⁶⁴, A. Shires⁹, R. Silva Coutinho⁴⁸, G. Simi²², M. Sirendi⁴⁷, N. Skidmore⁴⁶, I. Skillicorn⁵¹, T. Skwarnicki⁵⁹, N.A. Smith⁵², E. Smith^{55,49}, E. Smith⁵³, J. Smith⁴⁷, M. Smith⁵⁴, H. Snoek⁴¹, M.D. Sokoloff⁵⁷, F.J.P. Soler⁵¹, F. Soomro³⁹, D. Souza⁴⁶, B. Souza De Paula², B. Spaan⁹, P. Spradlin⁵¹, S. Sridharan³⁸, F. Stagni³⁸, M. Stahl¹¹, S. Stahl¹¹, O. Steinkamp⁴⁰, O. Stenyakin³⁵, F. Sterpka⁵⁹, S. Stevenson⁵⁵, S. Stoica²⁹, S. Stone⁵⁹, B. Storaci⁴⁰, S. Stracka^{23,t}, M. Straticiuc²⁹, U. Straumann⁴⁰, R. Stroili²², L. Sun⁵⁷, W. Sutcliffe⁵³, K. Swientek²⁷, S. Swientek⁹, V. Syropoulos⁴², M. Szczekowski²⁸, P. Szczypka^{39,38}, T. Szumlak²⁷, S. T'Jampens⁴, M. Teklishyn⁷, G. Tellarini^{16,f}, F. Teubert³⁸, C. Thomas⁵⁵, E. Thomas³⁸, J. van Tilburg⁴¹, V. Tisserand⁴, M. Tobin³⁹, J. Todd⁵⁷, S. Tolk⁴², L. Tomassetti^{16,f}, D. Tonelli³⁸, S. Topp-Joergensen⁵⁵, N. Torr⁵⁵, E. Tournefier⁴, S. Tourneur³⁹, M.T. Tran³⁹, M. Tresch⁴⁰, A. Trisovic³⁸, A. Tsaregorodtsev⁶, P. Tsopelas⁴¹, N. Tuning⁴¹, M. Ubeda Garcia³⁸, A. Ukleja²⁸, A. Ustyuzhanin⁶⁴, U. Uwer¹¹, C. Vacca¹⁵, V. Vagnoni¹⁴, G. Valenti¹⁴, A. Vallier⁷, R. Vazquez Gomez¹⁸, P. Vazquez Regueiro³⁷, C. Vázquez Sierra³⁷, S. Vecchi¹⁶, J.J. Velthuis⁴⁶, M. Veltri^{17,h}, G. Veneziano³⁹, M. Vesterinen¹¹, B. Viaud⁷, D. Vieira², M. Vieites Diaz³⁷, X. Vilasis-Cardona^{36,p}, A. Vollhardt⁴⁰, D. Volyansky¹⁰, D. Voong⁴⁶, A. Vorobyev³⁰, V. Vorobyev³⁴, C. Vöß⁶³, J.A. de Vries⁴¹, R. Waldi⁶³, C. Wallace⁴⁸, R. Wallace¹², J. Walsh²³, S. Wandernoth¹¹, J. Wang⁵⁹, D.R. Ward⁴⁷, N.K. Watson⁴⁵, D. Websdale⁵³, M. Whitehead⁴⁸, D. Wiedner¹¹, G. Wilkinson^{55,38}, M. Wilkinson⁵⁹, M.P. Williams⁴⁵, M. Williams⁵⁶, H.W. Wilschut⁶⁶, F.F. Wilson⁴⁹, J. Wimberley⁵⁸, J. Wishahi⁹, W. Wislicki²⁸, M. Witek²⁶, G. Wormser⁷, S.A. Wotton⁴⁷, S. Wright⁴⁷, K. Wyllie³⁸, Y. Xie⁶¹, Z. Xing⁵⁹, Z. Xu³⁹, Z. Yang³, X. Yuan³, O. Yushchenko³⁵, M. Zangoli¹⁴, M. Zavertyaev^{10,b}, L. Zhang³, W.C. Zhang¹², Y. Zhang³, A. Zhelezov¹¹, A. Zhokhov³¹, L. Zhong³.

¹ Centro Brasileiro de Pesquisas Físicas (CBPF), Rio de Janeiro, Brazil

² Universidade Federal do Rio de Janeiro (UFRJ), Rio de Janeiro, Brazil

³ Center for High Energy Physics, Tsinghua University, Beijing, China

⁴ LAPP, Université de Savoie, CNRS/IN2P3, Annecy-Le-Vieux, France

⁵ Clermont Université, Université Blaise Pascal, CNRS/IN2P3, LPC, Clermont-Ferrand, France

⁶ CPPM, Aix-Marseille Université, CNRS/IN2P3, Marseille, France

⁷ LAL, Université Paris-Sud, CNRS/IN2P3, Orsay, France

⁸ LPNHE, Université Pierre et Marie Curie, Université Paris Diderot, CNRS/IN2P3, Paris, France

⁹ Fakultät Physik, Technische Universität Dortmund, Dortmund, Germany

¹⁰ Max-Planck-Institut für Kernphysik (MPIK), Heidelberg, Germany

¹¹ Physikalisches Institut, Ruprecht-Karls-Universität Heidelberg, Heidelberg, Germany

¹² School of Physics, University College Dublin, Dublin, Ireland

¹³ Sezione INFN di Bari, Bari, Italy

¹⁴ Sezione INFN di Bologna, Bologna, Italy

¹⁵ Sezione INFN di Cagliari, Cagliari, Italy

¹⁶ Sezione INFN di Ferrara, Ferrara, Italy

¹⁷ Sezione INFN di Firenze, Firenze, Italy

¹⁸ Laboratori Nazionali dell'INFN di Frascati, Frascati, Italy

- ¹⁹ *Sezione INFN di Genova, Genova, Italy*
- ²⁰ *Sezione INFN di Milano Bicocca, Milano, Italy*
- ²¹ *Sezione INFN di Milano, Milano, Italy*
- ²² *Sezione INFN di Padova, Padova, Italy*
- ²³ *Sezione INFN di Pisa, Pisa, Italy*
- ²⁴ *Sezione INFN di Roma Tor Vergata, Roma, Italy*
- ²⁵ *Sezione INFN di Roma La Sapienza, Roma, Italy*
- ²⁶ *Henryk Niewodniczanski Institute of Nuclear Physics Polish Academy of Sciences, Kraków, Poland*
- ²⁷ *AGH - University of Science and Technology, Faculty of Physics and Applied Computer Science, Kraków, Poland*
- ²⁸ *National Center for Nuclear Research (NCBJ), Warsaw, Poland*
- ²⁹ *Horia Hulubei National Institute of Physics and Nuclear Engineering, Bucharest-Magurele, Romania*
- ³⁰ *Petersburg Nuclear Physics Institute (PNPI), Gatchina, Russia*
- ³¹ *Institute of Theoretical and Experimental Physics (ITEP), Moscow, Russia*
- ³² *Institute of Nuclear Physics, Moscow State University (SINP MSU), Moscow, Russia*
- ³³ *Institute for Nuclear Research of the Russian Academy of Sciences (INR RAN), Moscow, Russia*
- ³⁴ *Budker Institute of Nuclear Physics (SB RAS) and Novosibirsk State University, Novosibirsk, Russia*
- ³⁵ *Institute for High Energy Physics (IHEP), Protvino, Russia*
- ³⁶ *Universitat de Barcelona, Barcelona, Spain*
- ³⁷ *Universidad de Santiago de Compostela, Santiago de Compostela, Spain*
- ³⁸ *European Organization for Nuclear Research (CERN), Geneva, Switzerland*
- ³⁹ *Ecole Polytechnique Fédérale de Lausanne (EPFL), Lausanne, Switzerland*
- ⁴⁰ *Physik-Institut, Universität Zürich, Zürich, Switzerland*
- ⁴¹ *Nikhef National Institute for Subatomic Physics, Amsterdam, The Netherlands*
- ⁴² *Nikhef National Institute for Subatomic Physics and VU University Amsterdam, Amsterdam, The Netherlands*
- ⁴³ *NSC Kharkiv Institute of Physics and Technology (NSC KIPT), Kharkiv, Ukraine*
- ⁴⁴ *Institute for Nuclear Research of the National Academy of Sciences (KINR), Kyiv, Ukraine*
- ⁴⁵ *University of Birmingham, Birmingham, United Kingdom*
- ⁴⁶ *H.H. Wills Physics Laboratory, University of Bristol, Bristol, United Kingdom*
- ⁴⁷ *Cavendish Laboratory, University of Cambridge, Cambridge, United Kingdom*
- ⁴⁸ *Department of Physics, University of Warwick, Coventry, United Kingdom*
- ⁴⁹ *STFC Rutherford Appleton Laboratory, Didcot, United Kingdom*
- ⁵⁰ *School of Physics and Astronomy, University of Edinburgh, Edinburgh, United Kingdom*
- ⁵¹ *School of Physics and Astronomy, University of Glasgow, Glasgow, United Kingdom*
- ⁵² *Oliver Lodge Laboratory, University of Liverpool, Liverpool, United Kingdom*
- ⁵³ *Imperial College London, London, United Kingdom*
- ⁵⁴ *School of Physics and Astronomy, University of Manchester, Manchester, United Kingdom*
- ⁵⁵ *Department of Physics, University of Oxford, Oxford, United Kingdom*
- ⁵⁶ *Massachusetts Institute of Technology, Cambridge, MA, United States*
- ⁵⁷ *University of Cincinnati, Cincinnati, OH, United States*
- ⁵⁸ *University of Maryland, College Park, MD, United States*
- ⁵⁹ *Syracuse University, Syracuse, NY, United States*
- ⁶⁰ *Pontifícia Universidade Católica do Rio de Janeiro (PUC-Rio), Rio de Janeiro, Brazil, associated to ²*
- ⁶¹ *Institute of Particle Physics, Central China Normal University, Wuhan, Hubei, China, associated to ³*
- ⁶² *Departamento de Física, Universidad Nacional de Colombia, Bogota, Colombia, associated to ⁸*
- ⁶³ *Institut für Physik, Universität Rostock, Rostock, Germany, associated to ¹¹*
- ⁶⁴ *National Research Centre Kurchatov Institute, Moscow, Russia, associated to ³¹*
- ⁶⁵ *Instituto de Física Corpuscular (IFIC), Universitat de Valencia-CSIC, Valencia, Spain, associated to ³⁶*
- ⁶⁶ *Van Swinderen Institute, University of Groningen, Groningen, The Netherlands, associated to ⁴¹*
- ⁶⁷ *Celal Bayar University, Manisa, Turkey, associated to ³⁸*

- ^a *Universidade Federal do Triângulo Mineiro (UFMT), Uberaba-MG, Brazil*
- ^b *P.N. Lebedev Physical Institute, Russian Academy of Science (LPI RAS), Moscow, Russia*
- ^c *Università di Bari, Bari, Italy*
- ^d *Università di Bologna, Bologna, Italy*
- ^e *Università di Cagliari, Cagliari, Italy*
- ^f *Università di Ferrara, Ferrara, Italy*
- ^g *Università di Firenze, Firenze, Italy*
- ^h *Università di Urbino, Urbino, Italy*
- ⁱ *Università di Modena e Reggio Emilia, Modena, Italy*
- ^j *Università di Genova, Genova, Italy*
- ^k *Università di Milano Bicocca, Milano, Italy*
- ^l *Università di Roma Tor Vergata, Roma, Italy*
- ^m *Università di Roma La Sapienza, Roma, Italy*
- ⁿ *Università della Basilicata, Potenza, Italy*
- ^o *AGH - University of Science and Technology, Faculty of Computer Science, Electronics and Telecommunications, Kraków, Poland*
- ^p *LIFAELS, La Salle, Universitat Ramon Llull, Barcelona, Spain*
- ^q *Hanoi University of Science, Hanoi, Viet Nam*
- ^r *Università di Padova, Padova, Italy*
- ^s *Università di Pisa, Pisa, Italy*
- ^t *Scuola Normale Superiore, Pisa, Italy*
- ^u *Università degli Studi di Milano, Milano, Italy*
- ^v *Politecnico di Milano, Milano, Italy*